journal of the mechanical behavior of biomedical materials 136 (2022) 105474

Contents lists available at ScienceDirect

Journal of the Mechanical Behavior of Biomedical Materials

journal homepage: www.elsevier.com/locate/jmbbm

Rheological characterization of cell-laden alginate-gelatin hydrogels for 3D biofabrication

Tyler Gregory, Prateek Benhal, Annie Scutte, David Quashie Jr., Kiram Harrison, Casey Cargill, Saliya Grandison, Mary Jean Savitsky, Subramanian Ramakrishnan **, Jamel Ali *

Department of Chemical and Biomedical Engineering, FAMU-FSU College of Engineering, Tallahassee, FL, 32310, USA

ARTICLE INFO

Keywords:
3D Biofabrication
Hydrogel rheology
3D Bioprinting
Biomaterials
and Tissue microenvironment

ABSTRACT

Biofabrication of tissue models that closely mimic the tumor microenvironment is necessary for high-throughput anticancer therapeutics. Extrusion-based bioprinting of heterogeneous cell-laden hydrogels has shown promise in advancing rapid artificial tissue development. A major bottleneck limiting the rapid production of physiologically relevant tissue models is the current limitation in effectively printing large populations of cells. However, by significantly increasing hydrogel cell-seeding densities, the time required to produce tissues could be effectively reduced. Here, we explore the effects of increasing cell seeding densities on the viscoelastic properties, printability, and cell viability of two different alginate-gelatin hydrogel compositions. Rheological analysis of hydrogels of varying cell seeding densities reveals an inverse relationship between cell concentration and zero-shear viscosity. We also observe that as cell seeding densities increases, the storage moduli decrease, thus lowering the required printing pressures for gel extrusion. We also observe that increasing cell concentration can negatively impact the structural properties of the extruded material by increasing post-print line spreading. We find that hydrogels composed of higher molecular weight alginates and the highest cell-seeding densities (10^7 cells/mL) yield higher cell viability (>80%) and structural uniformity after printing. The optimized printing parameters determined for the alginate-gelatin bioinks explored may aid in the future rapid fabrication of functional tissue models for therapeutic screening.

1. Introduction

A major focus of current regenerative medicine is aimed at developing engineered artificial tissues to replace damaged tissues and restore normal physiological functions (Moroni et al., 2018). There is a significant discrepancy in the availability and demand for organ transplantation, which attributes to various factors such as cost, organ preservation, and patient immune rejection (Ahadian and Khademhosseini, 2018; Ochando et al., 2017; Pedde et al., 2017). Achieving regenerative alternatives to bridge the gap between donors and recipient tissues requires an understanding of the complexity of cells and their dynamic extracellular matrix (Mota et al., 2020). In addition to transplantable organs, engineered tissues are essential for many applications, such as high-throughput drug screening for cancer therapies (Ahadian and Khademhosseini, 2018). Despite efforts to develop viable *in vitro* produced nonimmunogenic tissues for transplantation, mimicking the complexity of the physiological microenvironment remains a challenge.

Traditionally, *in vitro* tissue models have utilized two-dimensional (2D) surfaces, such as plastic and glass chambers, where monolayers of adherent cells form (Hickman et al., 2014; Moysidou et al., 2021). Despite the ease and convenience of 2D culture models, these systems fail to recapitulate natural tissues due to the lack of complexity inherent in the physiological tissue environment. The 2D derived tissue models often lack complex structural architectures necessary to promote biochemical and biophysical cues for cell mechanosensing and communication, vital to native processes (Jensen and Teng, 2020; Kapalczynska et al., 2018; Mandrycky et al., 2016). Various techniques have been used to induce cell morphological changes in 2D cultures, making them closer to native tissues. These techniques include sandwich cultures, micropatterning, and alternating substrate stiffness (Duval

* Corresponding author.
** Corresponding author.
E-mail addresses: tyler1.gregory@famu.edu (T. Gregory), prateekbg@gmail.com (P. Benhal), annie1.scutte@famu.edu (A. Scutte), david1.quashie@famu.edu (D. Quashie), kiram1.harrison@famu.edu (K. Harrison), crc19p@fsu.edu (C. Cargill), sgrandison@fsu.edu (S. Grandison), maryjean1.savitsky@famu.edu (M.J. Savitsky), srama@eng.famu.fsu.edu (S. Ramakrishnan), jali@eng.famu.fsu.edu (J. Ali).

https://doi.org/10.1016/j.jmbbm.2022.105474
Received 18 April 2022; Received in revised form 3 September 2022; Accepted 18 September 2022
Available online 22 September 2022

et al., 2017). However, these methods can add layers of complexity and cost to the development and maintenance of 2D cultures, eliminating some of the previous mentioned benefits. The limitations of 2D tissue-derived models have paved the way for the transition to three-dimensional (3D) tissue models to capture the tissue microenvironment's complexity. More advanced fabrication methods have been established to create more realistic culture environments that can more closely mimic the conditions found in various native tissues (Hickman et al., 2014).

The emergence of biofabrication technologies, such as 3D bioprinting, has enabled the development of complex 3D biological constructs engineered to embed specialized functions (Moroni et al., 2018). Biofabrication of artificial tissue allows for *in vitro* models that have a variety of applications, from drug screening to tissue regeneration. The fabrication process of tissues generally involves carefully creating scaffolds that can facilitate cellular attachment and proliferation and remain physically stable until cells are self-sufficient. In tissue engineering, it is vital to fine-tune the characteristics of biomaterials to ensure that microenvironments promote *in vitro* physiological processes that occur *in vivo* (Baker and Chen, 2012). Cells respond to various cues in their extracellular environment, including biochemical and biomechanical signals. These factors are essential for survivability and behavior (Discher et al., 2005; Wong et al., 2004). Careful consideration is needed when deciding the materials to use when creating artificial tissues, including the scaffold biomaterial and the required cell types to recapitulate *in vivo* tissues (Shafiee and Atala, 2016).

Bioprinting allows for precise control over the spatial arrangements of cells, biomaterials, and active biological factors. Precision in cell distribution within engineered constructs is essential for mimicking the complexity of the tissue microenvironment. One of the most critical components in 3D biofabrication is the biomaterial selected to house cells (Moroni et al., 2018). Biomaterials can be synthetically or naturally derived and should be biocompatible, biodegradable, and non-immunogenic. Biomaterials should also have properties, such as viscoelasticity, which match natural tissues and are compatible with the desired fabrication technique. One of the most commonly used biofabrication techniques is extrusion-based bioprinting. Extrusion-based bioprinting requires materials to exhibit shear thinning behavior with rapid stabilization upon deposition (Moroni et al., 2018). The most widely used natural polymers to formulate shear-thinning hydrogels for extrusion-based printing are collagen, gelatin, silk, and alginate. These materials can be engineered to exhibit biochemical and biophysical cues typically present in native extracellular matrix.

Alginate is often chosen as a scaffolding material in various biofabrication methods because of several factors: inexpensiveness, availability, biocompatibility, and tuneability. Alginates are natural, nonimmunogenic, linear biopolymers derived from brown algae or bacterial sources. Alginate consists of 1,4-linked Beta-D-mannuronic acid (M) and 1,4 Alpha-L-guluronic acid (G) residues arranged in homogeneous or heterogeneous block patterns (Axpe and Oyen, 2016; Rastogi and Kandasubramanian, 2019; Szekalska et al., 2016). The molecular weight and distribution of M and G blocks are key factors contributing to the physicochemical properties of alginates, such as viscosity and sol-gel transition (Axpe and Oyen, 2016; Kuo and Ma, 2001; Szekalska et al., 2016). Alginates are crosslinked using divalent ions such as Ca^{2+} and Ba^{2+}. The degree of alginate crosslinking can be controlled by varying the exposure time and concentration of the crosslinking agent. Alginates are typically mixed in various ratios with other natural polymers such as gelatin, collagen, or chitosan to enhance bioinks viscoelastic and mechanical properties (Kuo and Ma, 2001). Gelatin is commonly used with alginate as it can improve thermal crosslinking of the hydrogel at room temperature, increasing the mechanical properties of gels (Rastogi and Kandasubramanian, 2019).

One of the main challenges with fabricating 3D constructs is achieving high cell seeding densities (Leberfinger et al., 2019). High cell seeding densities, concentrations greater than 10^6 cell/mL, are necessary to decrease the time it takes for cells to proliferate and differentiate when encapsulated in 3D environments (Zhang et al., 2020). Recent investigations have demonstrated the limitations of high cell seeding densities and extrusion-based bioprinting, however there is no clearly defined relationship between cell seeding density and the printability of the bioinks (Diamantides et al., 2019; Gillispie et al., 2020; Schwartz et al., 2020). The most frequently used cell seeding density is commonly around 1×10^6 cells/mL. Cell seeding concentrations are also known to directly affect cell survivability. For example, cell seeding densities below 10^6 cells/mL have high viability but a reduced likelihood of tissue maturation. However, cell seeding densities above 10^6 cells/mL have often led to increased cell-to-cell interactions and raised the possibility of hypoxia within printed structures. Higher cell seeding densities also require more media and supplementation to maintain growth (Mauck et al., 2003). Seeding densities as high as 1×10^8 cells/mL have been printed with success and high cell viability, though the printing method here was laser-assisted bioprinting (Guillotin et al., 2010; Holzl et al., 2016). Cell-to-cell interactions vary between cell types and can affect a hydrogel's printability depending on the printed cells and ink. Similar printability trends are observed for different hydrogels and seeding densities, regardless of cell type (Schwartz et al., 2020).

Here, we examine the effect of cell seeding densities on the viscoelastic properties, cell viability, and printability of two types of alginate-based hydrogels. The sodium alginates used in this investigation are of two different molecular weights. We aim to expand on the previously reported mechanical data (Di Giuseppe et al., 2018) for these widely used hydrogels to enable the rapid additive manufacturing of tissues. Specifically, the results presented here identify a relationship between increasing cell seeding density and the viscoelastic properties of two types of alginate-based gels. The relationship identified aid in defining printing parameters for producing bioinks with varying alginate composition and cell densities. We also explore the effects of cell seeding on hydrogel printability and cell viability. Bioink viscoelastic properties, printability, and cell viability are affected by increasing cell seeding densities, which vary based on the molecular weight of alginate.

2. Methods

2.1. Materials and preparation

The hydrogel materials in this investigation were alginate, obtained from MilliporeSigma (Alginic acid sodium salt, low viscosity (Catalog #: A2033), and medium viscosity (Catalog #: A1112)), with gelatin, obtained from Acros Organics (Gelatin type A), PBS (pH 7.4), and calcium chloride ($CaCl_2$, granular). The low viscosity alginate had a molecular weight of 24 kDa (low MW), and the medium viscosity alginate had a molecular weight of 773 kDa (high MW). Hydrogels used had a final composition of 3% alginate (w/v) and 4% gelatin (w/v). The components used to produce the hydrogels are low and medium viscosity powdered alginate (Sigma Aldrich), type A gelatin, and Dulbecco's Modified Eagle Medium (DMEM). Alginate and gelatin powders were weighed, and UV sterilized in a biological safety cabinet for 30 min. Once sterilized, the gelatin powder was mixed in DMEM media at 50 °C and 400 rpm for 1 h. Then, the alginate powder was then added to the gelatin-DMEM mixture (Fig. 1) to mix at 50 °C and 400 rpm for 3 h. Once a homogenized solution was obtained, the hydrogel precursors (uncrosslinked hydrogels) were centrifuged for 5 min at 850 rcf to remove bubbles. After degassing, the hydrogels were stored at 4 °C °until use (Fig. 1A).

2.2. Hydrogel compositions

In this research investigation, two different molecular weights of alginic acid sodium salt (24 kDa and 773 kDa) were used to produce alginate-gelatin hydrogels. The composition used for both types of

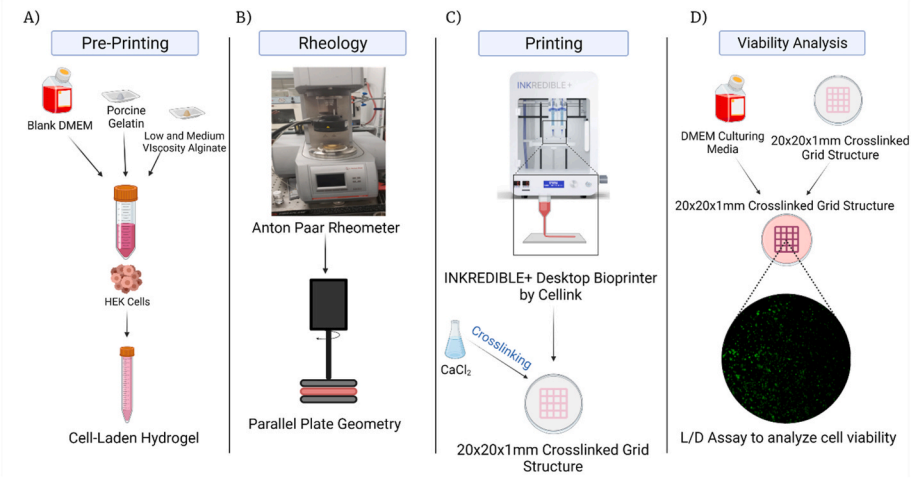

Fig. 1. Rheological characterization and fabrication of cell-laden alginate-based hydrogels. (A) Schematic of hydrogels formulation using DMEM cell culture media, gelatin, and low or high MW alginate incorporating HEK 293 cells at varying concentrations. (B) rheological characterization of hydrogel samples an Anton Paar MCR302 rheometer. (C) Schematic of extrusion-based fabrication of alginate-based scaffolds in a lattice pattern crosslinked with 5% $CaCl_2$ solution. (D) Live/Dead viability assay of cell-laden alginate-based scaffold post-fabrication.

hydrogels were 3% alginate (w/v) and 4% gelatin(w/v). The cell seeding densities used were 0, 2×10^5, 1.5×10^6, and 2×10^7 cells/ml.

2.3. Rheology

Rheological measurements were obtained using an Anton Paar rheometer with a 25 mm diameter parallel plate geometry. Samples were loaded onto the bottom plate of the rheometer at 37 °C before lowering the geometry to have a gap of 1 mm with the bottom base plate. After lowering the geometry, the samples were cooled to 17 °C to gelate samples, allowing the excess sample to be trimmed. The bottom plate temperature was then increased to 25 °C, where the sample was left to equilibrate for 20 min. Once the samples were equilibrated, the samples were subjected to various measurement profiles. First, oscillation measurements determined the storage modulus over a time period of 120 s with an amplitude gamma of 0.1% and a frequency of 1 Hz. Next, the storage modulus was measured as a function of frequency. Next, oscillation measurements were performed with an amplitude gamma of 0.1% and frequency ranging from 0.05 to 16 Hz. Viscosity and shear stress as a function of shear rate was measured. The shear rate was set to 1-50 s^{-1} with point durations from 3 to 20 s (Fig. 1B). The shear stress vs. shear rate graphs (Fig. 2C) were used to determine the dynamic yield stress by fitting the Herschel-Buckley model to the data with the following equation:

$$\sigma = K\dot{\gamma}^n + \sigma_o \quad (1)$$

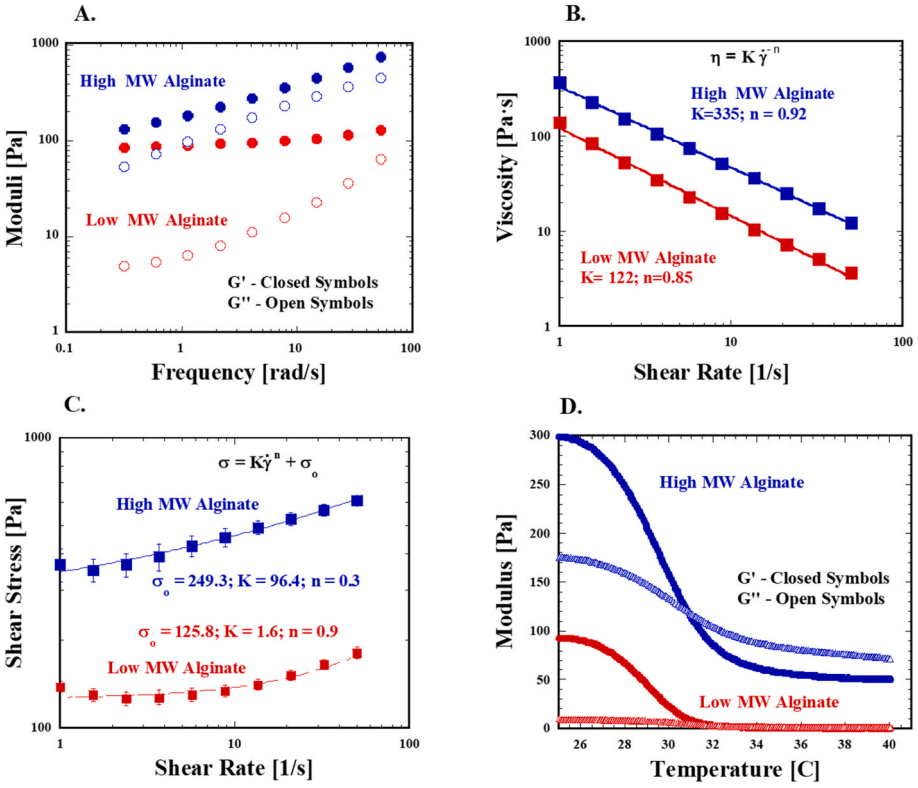

Fig. 2. Rheological characterization of uncrosslinked alginate-based hydrogels with varying molecular weight. (A) Frequency sweep of hydrogels from 0.34 to 100.53 rad/s at a constant amplitude gamma of 0.1%. (B) Viscosity as a function of shear rate, from 1 to 50 s^{-1}. (C) Shear stress as a function of shear rate, from 1 to 50 s^{-1}. (D) Temperature sweep from 25 to 40 °C.

where σ is shear stress, $\dot{\gamma}$ is shear rate, K is the consistency coefficient, n is the flow behavior index, and σ_o is the dynamic yield stress.

Crosslinking data was determined *via* oscillation measurements to determine the storage modulus over a time period of 120 s with an amplitude of 0.1% and a frequency of 1 Hz at 25 °C parallel plate. Next, the crosslinking solution, composed of 5% (w/v) $CaCl_2$, was added to the bowl after 120s. The sample was left to crosslink for an additional 180 s. The crosslinking solution was removed from the bowl and the sample was washed four times and submerged in 1xPBS solution. The sample was left submerged in the PBS solution for 420 s. The temperature of the sample was then increased to 37 °C over a time period of 1800 s with an amplitude gamma of 0.1% and a frequency of 1 Hz (Fig. 3).

To determine the molecular weight of the two alginate types, we used a 1.1° cone and plate geometry. Water-alginate solutions were made at varying concentrations. Alginate concentrations for the low viscosity alginate samples were 1 wt%, 0.75 wt%, 0.5 wt% and 0.25 wt %. Concentrations for the high MW alginate were 0.01 wt%, 0.005 wt%, 0.0025 wt%, and 0.00125 wt%. A volume of 1 mL of the solution was loaded to the bottom plate of the rheometer before lowering the cone. All measurements were carried out at 25 °C. The viscosity vs. shear measurements was conducted from 1 to 100 (1/s). The viscosity value at the linear region of the resulting graphs was then used to determine the intrinsic viscosity. The parameter values used to determine the final molecular weight were previously determined (Masuelli and Illanes, 2014).

2.4. Printing

2.4.1. Printing setup

The hydrogels were printed using a Cellink Inkredible + Bioprinter (CELLINK, Boston, MA). The Inkredible+ is a pneumatic extrusion-based bioprinter, that uses Cellink's HeartWare software for operation. The printer features an XYZ stage with a pneumatic pressure-controlled dispensing module, a fan chamber with a HEPA filter, and a temperature-controlled sleeve for the cylindrical nozzle. Hydrogels are loaded into cylindrical nozzles for printing. First, a piston was added to a cylindrical nozzle. Using a 3 ml syringe and a Luer-lock syringe coupler, the air was removed from the cylinder, forcing the piston to the bottom of the syringe. Next, hydrogels were heated to 37 °C before extracting with a 3 mL sterile syringe. Using a Luer lock coupler, the hydrogel was transferred into a cylindrical nozzle and capped. The nozzle was then placed in the Inkredible + printing sleeve (set to 25 °C). The nozzle was left to sit for 1.5 h, allowing the gel to equilibrate. After the hydrogel equilibrated, the nozzle cap was then replaced with a 0.41 mm ID tapered nozzle tip (Fig. 1C). Model *.STL files were sliced to have an infill density of 40% with a rectilinear infill pattern.

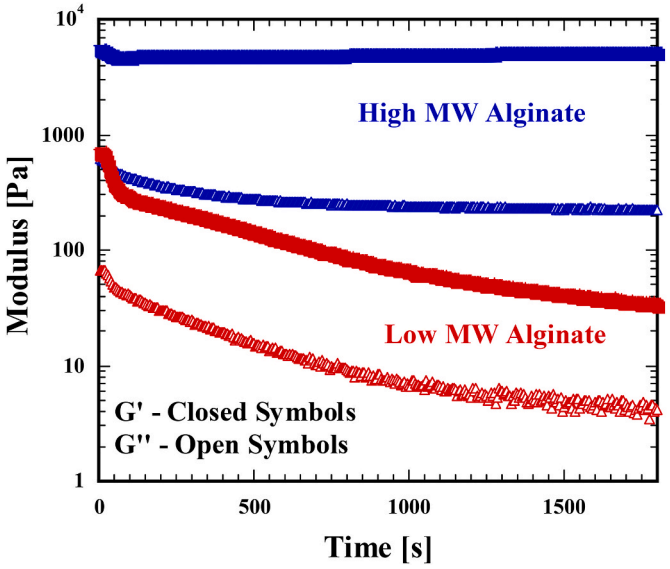

Fig. 3. Oscillatory shear measurements for hydrogels composed of high and low MW alginates. Measurements were obtained at a constant frequency of 1 Hz at 37 °C, after crosslinking with 5% $CaCl_2$.

2.4.2. Printing parameters

All hydrogel samples were printed in consecutive 20 mm parallel lines and 20 × 20 mm lattice patterns to determine each hydrogel sample's printing parameters. The parameters investigated were printing pressure (controlled by pneumatic pressure), and printing speed (controlled by the velocity of the nozzle tip). A lattice shape was chosen because it is conducive to determining printability factor (Pr) value, by finding the area of the empty pours that are printed. Images of the hydrogel prints were analyzed in ImageJ 1.53c. The line widths and uniformity were determined using the ImageJ line tool and averaged over four different line segments. The gels were printed in two-layer lattice structures to assess the pore area and the Pr value (Ouyang et al., 2016). The Pr value was determined using the following equation:

$$Pr = \frac{L^2}{16A} \tag{2}$$

Where, L represents the perimeter of the pores, and A represents the area of the pores. This equation also used to determine the shape and uniformity of the pores.

2.5. Cell culture

2.5.1. 2D cell culture

Immortalized human embryonic kidney (HEK 293) cells were obtained from American Type Culture Collection (ATCC). The HEK cells were cultured in Dulbecco's modified Eagle's medium (DMEM), supplemented with high glucose (4500 mg/L), L-glutamine, sodium pyruvate, 10% fetal bovine serum, and 2% penicillin-streptomycin. Cells were incubated at 37 °C in a humidified incubator at 5% CO_2. Cells were grown in tissue culture dishes and passaged when they reached confluency. The media was removed, and fresh media was added to the cultures every other day.

2.5.2. Cell encapsulation

Cells were incorporated into hydrogels when the culture dish reached >95% confluency. First, media was removed from confluent plates and washed with PBS at 37 °C. Then, the cells were detached from the cell culture plate by adding 2 mL of trypsin EDTA for 2 min. The cells were then suspended 0.5 ml (in 35 mm tissue treated dishes) or 2 mL (in 100 mm tissue treated dishes) of fresh media to create a stock solution of cells. The concentration of the stock solution was determined with the Countess II Automated Cell Counter (Thermo Fisher Scientific, Waltham, MA), allowing the approximate number of cells to be calculated. When the appropriate number of cells was achieved for the final concentration of the desired hydrogel (2×10^5, 1.5×10^6, and 2.1×10^7 cells/mL), trypsinized cells were then centrifuged, using the Eppendorf Centrifuge 5424 R (Eppendorf, Hamburg, Germany) at 850 rcf for 3 min. The cell pellet that was formed was then re-suspended in 25 μ L of media to create a highly concentrated stock solution. The stock solution is then added and mixed into a pre-heated (37 °C) sample of the hydrogel at an appropriate volume. The sample was gently mixed with manual stirring and aspiration while the gel was warm to reduce the shear stresses on the cells. The cell-laden hydrogels were then loaded into a 3 mL syringe for printing.

2.5.3. Printed structure preparation

The 3D cultures were made using two methods: one method for making hydrogel disks and printing into lattice structures. To form a

hydrogel disk, cell-laden hydrogel, at 37 °C, was manually deposited, in a dropwise fashion, onto the bottom of a culture dish with an approximate volume of 50 μ L. The drops were then cooled in a refrigerator at 4 °C for 3–5 min to allow the hydrogels to gel. The drops were then removed from the refrigerator and quickly submerged in 5% $CaCl_2$ for 3 min to crosslink the hydrogel. After 3 min, the $CaCl_2$ solution was aspirated from the culture dish, and the crosslinked hydrogel disks were then washed twice with sterile phosphate-buffered saline (1 × PBS). After rinsing the discs with PBS, DMEM media was added to the culture dishes and then incubated at 5% CO_2 at 37 °C. To make the cell-laden lattice structure, the cell-laden hydrogel was added to a 3D printing syringe, and the hydrogels were printed at 25 °C and a printing speed of 5 mm/s. After, printing the cell-laden hydrogel was submerged in $CaCl_2$ for 3 min and washed twice with sterile PBS. The printed constructs were then supplemented with media and incubated for five days. Cell media was exchanged with fresh media every two days.

2.6. 3D culture viability

The viability of the 3D cultures was assessed using Live/Dead viability assays (LDA) based on Calcein AM and Ethidium homodimer-1 (EthD-1). The LDA stock solutions were prepared by adding a 1: 10 μ l ratio of EthD-1 to Calcein AM to 1 ml of PBS in a microcentrifuge tube. The microcentrifuge tube was then covered with foil and vortexed for 5 min. The 3D culture of interest was transferred onto a glass slide for viewing. Then, the 3D culture was submerged in LDA solution for 45 min to stain the cells inside the disk. Once the cultures are stained, they were viewed under a fluorescent microscope. The samples were imaged using 4 ×, 20 ×, and 40 × objectives. Samples were imaged every day for 0–5 days. The images were then processed in ImageJ to obtain the viability of cells suspended in the hydrogel. Viability was determined by dividing the green fluorescence area by the total area of fluorescence (Fig. 1D).

2.7. Statistical analysis

Statistical analysis was conducted in Excel using two-way ANOVA statistical analysis. Experiments were performed in triplicate ($n = 3$) and significant differences at $p < 0.05$ (*) was used for statistical significance.

3. Results

3.1. Rheology

3.1.1. Non-cell laden hydrogels

The molecular weights for the low and high MW alginate used were determined to be 24 kDa and 773 kDa, respectively. As shown in Fig. 2, the molecular weight of alginate greatly impacts the viscoelastic properties of the formulated hydrogel precursor. We observed that the storage and loss modulus increases with increasing frequency and alginate molecular weight, but the relative difference in values between the storage and loss modulus is greatest for the low MW alginate-gelatin hydrogels (Fig. 2A). A crossover point where the loss modulus overtakes the storage modulus would be expected at higher frequencies, suggesting the low MW alginate hydrogels flow easier than the high MW hydrogels. The hydrogels also exhibit shear-thinning behavior where high MW alginate viscosity is three times the viscosity of the low MW alginate (Fig. 2B). Alginate-gelatin hydrogels are known to exhibit shear-thinning behavior. The greater viscosity and moduli of the high MW alginate are consistent with what would be expected with a polymer of greater size, likely allowing for a greater degree of physical crosslinking. By fitting the Herschel-Bulkley model to the data in Fig. 2C, we were able to calculate the dynamic yield stress for the low and high MW hydrogel precursors, 125.8 and 249.3 Pa*s, respectively (Fig. 2C). Taking into consideration the temperature sensitivity of alginate inks, temperature sweep tests were carried out to determine the gelation points of the two hydrogels. The crossover points were determined to be 30.9 °C and 33.0 °C for the high and low MW alginate-gelatin hydrogel precursors, respectively (Fig. 2D).

Fig. 3 displays the mechanical properties of our alginate-gelatin hydrogels after crosslinking. When the hydrogels were submerged in a crosslinking agent (5% w/v $CaCl_2$), the moduli of the hydrogels increased over the crosslinking period (120 s). Once the crosslinking agent is removed the sample was left to sit for 480s, before the temperature was increased to 37 °C to simulate incubation of the sample. After the temperature of the crosslinked sample was increased to incubation temperatures (37 °C), the moduli of the hydrogels sharply decreased for the first 100 s. For the High MW hydrogel, the storage modulus began to slightly increase, over the measurement period. The loss modulus of the High MW hydrogels, slowly decreased over the same time. The storage and modulus for the Low MW hydrogels decreased over the measurement time, beneath the moduli for the uncrosslinked hydrogel (Fig. 3).

3.1.2. Cell-laden hydrogels

Graphs shown in Fig. 4 and Fig. 5 display a decrease in hydrogel storage and loss moduli with increasing cell seeding densities for both low and high MW alginates (Figs. 4A and 5A). Data also depicts an increase in hydrogel shear thinning behavior with increasing cell seeding densities (Figs. 4B and 5B). The hydrogel control sample (0 cells/mL) had the highest viscosity, while hydrogels with a seeded cell concentration of 2×10^7 cells/mL had the lowest. However, with a cell concentration of 1.5×10^6 cells/mL and 2×10^7 cells/mL concentrations, hydrogels had similar shear-thinning viscosity values. Furthermore, although viscosity values differed for hydrogel with control and 2×10^5 cells/mL, they exhibited similar values for storage modulus with increasing frequency. Similar trends are observed for both high and low MW hydrogels, where a monotonic decrease in both the viscosity and storage modulus of the hydrogels is observed with respect to increasing cell concentration.

The rheological tests were conducted on high and low MW alginate-gelatin hydrogels. The data displays a softening of the hydrogel with increasing seeding densities of cells (Fig. 5). Both high and low MW hydrogels experience the softening effect. We see a systematic decrease in both the viscosity and storage modulus of the hydrogels with respect to increasing cell concentration.

The high MW alginate storage moduli were approximately three times greater than that of the low viscosity alginate (Fig. 6). Increasing the cell seeding density in both the types of hydrogels displayed a systematic decrease in the storage modulus (Fig. 6). However, the storage moduli remained greater for the high MW alginate for all cell concentrations versus the low MW alginate gels. The bioinks displayed an inverse relationship between the cell concentration and viscosity. The cell seeding density had a greater statistical significance storage modulus of the high MW alginate compared to the low MW alginate gels.

3.2. Hydrogel gelation

With the encapsulation of cells within the hydrogels, the storage modulus decreases, and the gelation point occurs at a lower temperature. When adding cells to low MW alginate hydrogels, the hydrogel is under-gelated and can become too fluid-like to hold a printable structure (Fig. 7). Under-gelated hydrogels were defined by $Pr < 1$, which correlates to the formation of a droplet at the end of the nozzle tip when extruded. Under-gelation results in large degrees of spreading of the printed filament, fusion of touching gel sections, and inability to fabricate multi-layer constructs. Proper gelation is defined by a $Pr = 1$ which occurs when hydrogels form continuous filaments extruded. These filaments were achieved when printing with the high MW alginate-based hydrogels at 25 °C.

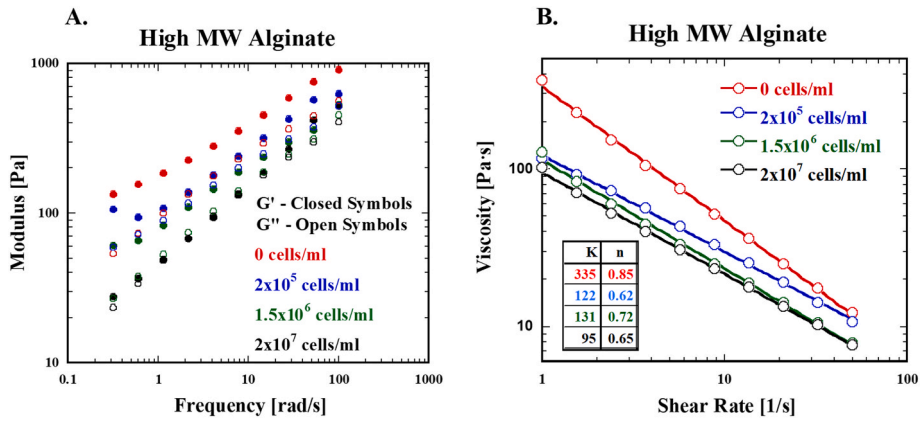

Fig. 4. Rheological characterization of cell-laden high MW alginate-based hydrogel with increasing cell seeding density. (A) Frequency sweep of cell-laden hydrogels from 0.34 to 100.53 rad/s at a constant amplitude gamma of 0.1% of four varying cell seeding densities: 0 cells/mL, 2×10^5 cells/mL, 1.5×10^6 cells/mL, and 2×10^7 cells/mL. (B) Viscosity as a function of shear rate from 1 to 50 s^{-1} displays the effects of cell seeding density on the hydrogel's shear-thinning behavior.

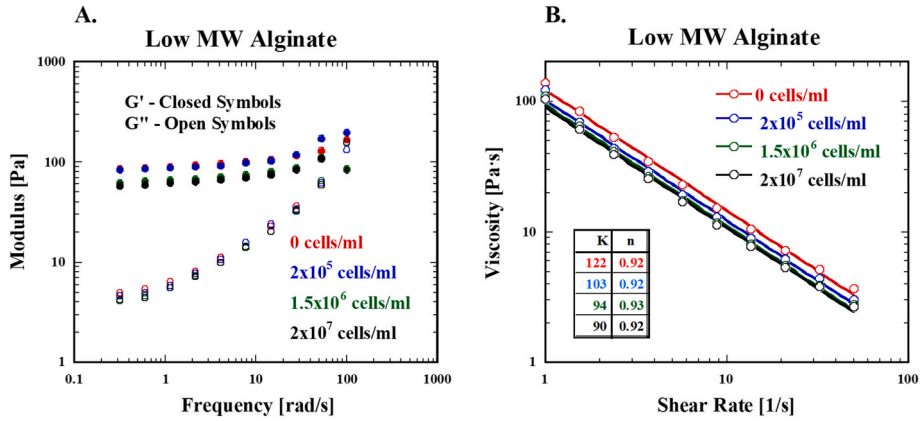

Fig. 5. Rheological characterization of cell-laden low-MW alginate-based hydrogel with increasing cell seeding density. (A) Frequency sweep of cell-laden hydrogels from 0.34 to 100.53 rad/s at a constant amplitude gamma of 0.1% of four varying cell seeding densities: 0 cells/mL, 2×10^5 cells/mL, 1.5×10^6 cells/mL, and 2×10^7 cells/mL. (B) Viscosity as a function of shear rate from 1 to 100 s^{-1} displays the effects of cell seeding density on the hydrogel's shear-thinning behavior.

3.3. Printing

Cell seeding density effects on printability with low MW alginate gels were evaluated. The low MW hydrogels were not able to print defined structures with cell concentrations above 2×10^5 cells/mL at printing temperatures of 25 °C due to under gelation. The high MW hydrogels did show increased line spreading in cell-laden hydrogels (Fig. 8). The high MW hydrogel with 1.5×10^6 cells/mL displayed the highest line spreading. The printing parameters necessary to print lines with the least amount of spreading changed with each seeding density. The control hydrogel was printed at 55 kPa and 4 mm/s, 2×10^5 cells/mL hydrogel was printed at 40 kPa and 6 mm/s, 1.5×10^6 cell/mL hydrogel was printed at 35 kPa and 6 mm/s, and 2×10^7 cells/mL hydrogel was printed at 25 kPa and 5 mm/s. Printing pressure needed to dispense the hydrogel decreased with the increase in the seeding density of the cell-laden hydrogels.

3.4. Viability

Fluorescent images of LIVE/DEAD stained HEK cells were examined to determine the viability of cells in crosslinked alginate-gelatin hydrogels over a five-day incubation period (Fig. 9C). Low MW alginates with high seeding densities were not printable at current printing conditions. The high MW alginate bioinks displayed high cell viability and reduced line spreading. The low MW samples of seeding densities of 2×10^5 and 2×10^7 cells/mL displayed high variation between the measurement days (Fig. 9A). The high MW sample of 1.5×10^6 cells/mL maintained stable viability (>80% viability) throughout the testing period, possibly due to less crowding of cells or less stress to cells when printing (Fig. 9B). This data suggests that while high MW alginate gels at a seeding density of 1.5×10^6 may have overall greater viability, however gels with a density of 2×10^7 cells/mL showed similar viability.

4. Discussion

Alginate and gelatin are the most commonly used biopolymers used for producing hydrogels for 3D bioprinting because of their availability, inexpensiveness, and biocompatibility (Axpe and Oyen, 2016). Several alginates are available for use in bioprinting applications, mainly differing in molecular weight and M/G blocks. Here, one of the aims was to examine the behavior of hydrogels composed of varying alginates that differ in printability and viability at varying cell seeding densities. This work lays the groundwork for determining printing parameters for the printing of varying MW alginate-gelatin hydrogels with cell seeding densities at varying orders of magnitude.

4.1. Effect of alginate molecular weight on hydrogel rheology

Based on the rheological data obtained, we have determined that the molecular weight of alginate plays an essential role in the pre-crosslinked properties of alginate-based hydrogels. The storage

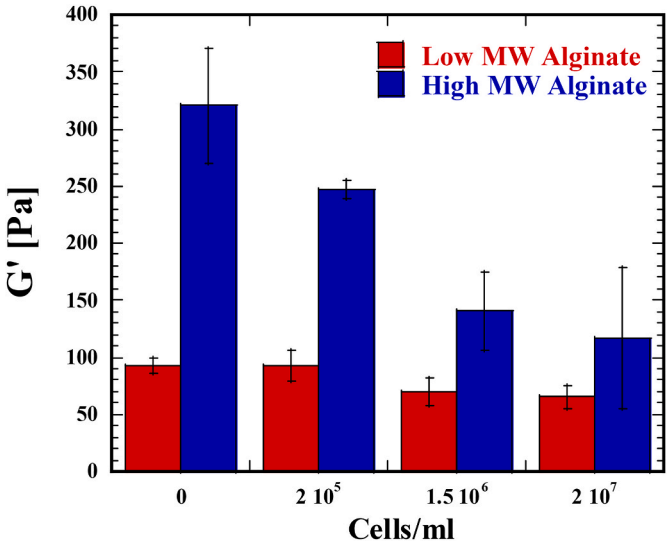

Fig. 6. The effects of alginate type and cell seeding density on the storage modulus of high and low Mw alginate-based hydrogels. (A) A plot of the storage modulus of hydrogels composed of different alginates and seeding densities at a constant frequency of 1Hz. All rheological data was obtained at 25 °C. There is a decrease in hydrogel storage modulus with increasing cell seeding density for both low and high MW alginate-based hydrogels.

modulus of the low MW alginate hydrogel was significantly lower than that of the high MW hydrogel, differing by approximately 230 Pa (Fig. 2). Previous studies have shown that the alginate's molecular weight plays a role in the viscoelastic properties observed (Szekalska et al., 2016). Though not directly measured, the low MW alginate appeared to have a longer gelation time than the high MW alginate. The high MW alginate created a stiffer gel with minimal spreading after printing. The stiffness of the high MW alginate was likely due to longer polymer lengths, leading to greater physical crosslinking within the hydrogel. The hydrogels with no cells were printable at room temperature; however, the high MW hydrogel required more pressure to extrude due to greater storage modulus and viscosity caused by the greater polymer length. Printing at higher pressures and viscosities of hydrogels leads to more significant stresses experienced by encapsulated cells. These shear forces can stress and damage cells, potentially decreasing viability after printing.

After extruding the hydrogels, the printed structures were crosslinked in order to maintain their shape in the incubator at 37 °C. The two hydrogels behaved differently after crosslinking. Both hydrogel precursors displayed increases in their storage modulus after being exposed to the crosslinking solution, but the storage modulus of the high MW alginate hydrogel increased to over an order of magnitude greater than the uncrosslinked hydrogel precursor storage modulus. The low MW hydrogel followed a similar pattern when crosslinking, but the storage modulus continued to decrease over the testing duration at 37 °C. The stiffness of the high MW hydrogels falls within range of previously reported crosslinked alginate-based hydrogels (Gonzalez-Fernandez et al., 2021; Mondal et al., 2019). The physical properties of the hydrogels remained within physiological relevant stiffnesses for both low and high MW samples (Vining and Mooney, 2017).

Cell behavior has been observed to change based on the stiffness of the matrix they inhabit (Vining and Mooney, 2017). Complete understating of the physiochemical interactions between cells and their microenvironment is currently lacking, however, changing the stiffness of the extracellular matrix has been shown to reliably determine some cellular behavior, such as differentiation in some cell types (El-Rashidy et al., 2021; Navaro et al., 2015; Ye et al., 2016; W. D. Zhang et al., 2020). One of the major challenges in 3D bioprinting is balancing the mechanical properties of the hydrogel with biocompatibility. Stiffer hydrogels have been observed to reduce the proliferation of cells but lead to greater printing outcomes (Bott et al., 2010; Ning et al., 2016). Since alginate-gelatin hydrogels are biodegradable, the stiffens of the hydrogel will decrease over the incubation period (Chung et al., 2013).

4.2. *Effect of initial seeding density on hydrogel rheology*

Increasing the initial seeding densities of mammalian cells within a hydrogel decreased the gel's stiffness and viscosity. This is likely because the cells in the hydrogel disrupt the matrix causing less physical crosslinking. We found that the increased cell densities had a more significant impact on the hydrogels composed of high MW alginate than the same cell seeding densities had on the low MW alginate. The viscosity and storage moduli did not directly correlate to the printability of the hydrogels. Still, they indicated the relative pressures that the gels would need to be printed to form a filament with minimal line spreading. The hydrogels composed of low MW alginates were not good candidates for printing at the selected conditions. The low MW alginate gels were soft and under-gelated when printing at 25 °C; however, these gels would likely be printable at lower temperatures (e.g., 18–20 °C), as alginate and gelatin stiffness and viscosity increase with decreasing temperatures.

Additionally, we discovered that increasing the initial seeding densities of the hydrogels decreased their viscosity, storage, and loss

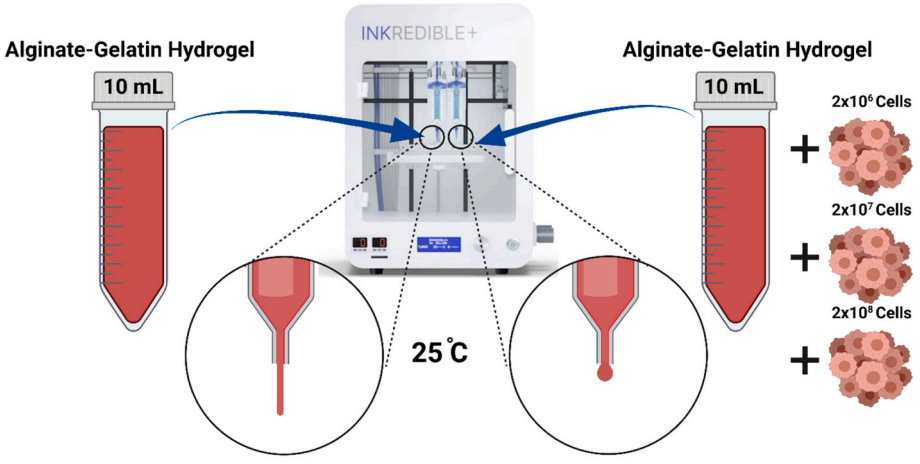

Fig. 7. Cell loading effects on hydrogel gelation. A schematic depicting the impact of the addition of cells on the gelation of hydrogels, thus affecting the hydrogel printability.

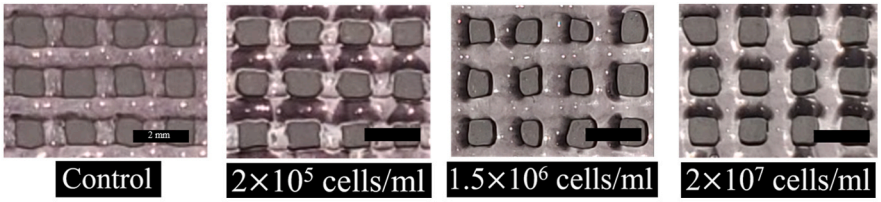

High MW Alg.	Area [mm^2]	Perimeter [mm]	Pr Value
Control	1.02 ± 0.14	3.87 ± 0.31	0.92 ± 0.03
2×10^5 cells/mL	0.78 ± 0.11	3.49 ± 0.32	0.98 ± 0.05
1.5×10^6 cells/mL	0.68 ± 0.12	3.13 ± 0.27	0.91 ± 0.02
2×10^7 cells/mL	0.88 ± 0.08	3.52 ± 0.17	0.88 ± 0.01

Fig. 8. Cell seeding density effects on hydrogel printability. The table depicts that adding cells to high MW alginate will increase hydrogel spreading. The images represent the best (lowest line width) print for each of the compositions of the cell-laden hydrogel. The printing parameters for the control hydrogel was 55 kPa and 4 mm/s; 2 × 10^5 cells/mL hydrogel was at 40 kPa and 6 mm/s; 1.5 × 10^6 cell/mL hydrogel was 35 kPa and 6 mm/s; and 2 × 10^7 cells/mL hydrogel was at 25 kPa and 5 mm/s. Scale bars are 2 mm.

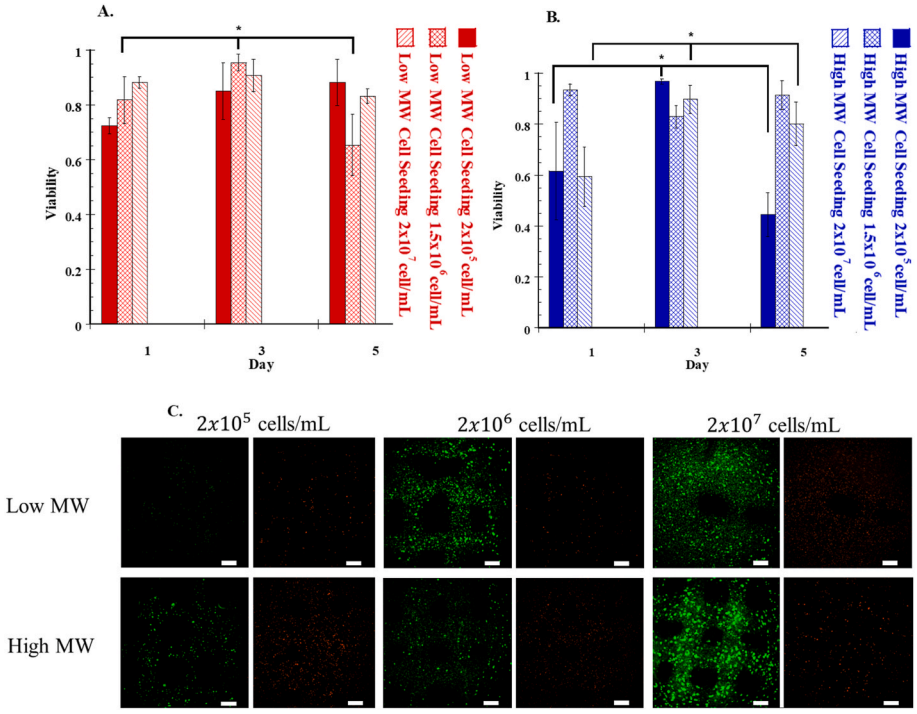

Fig. 9. Viability of HEK 293 in alginate-based hydrogels. (A) Viability of HEK 293 with increasing cell seeding densities in low-Mw alginate-based hydrogel scaffolds. (B) HEK 293 with increasing cell seeding densities in high-Mw alginate-based hydrogel scaffolds. Two-way ANOVA analysis determined the statistical significance at the $P < 0.05$ level represented by *. (C) Fluorescent images of cells, stained with a LIVE/DEAD staining solution, encapsulated within printed hydrogels. Images taken three day after printing (scale bar is 100 μm).

moduli. Consistent with previous findings, the hydrogel viscosity did not decrease linearly with increasing cell concentration. (Kiyotake et al., 2019). We suspect that this could be attributed to the cells within the hydrogel disrupting the microstructure of the gel to varying degrees. The polymer network of the high MW alginate appears to be able to maintain the internal matrix of the gel at high cell loading densities. The cells seeded in the hydrogel may have disrupted the matrix of the low MW alginate hydrogels to a greater extent and prevented gelation at room temperature, with similar seeding densities to that of high MW alginate hydrogels. The weaker network of the low MW alginate is believed to be disrupted to a greater extent by the presence of cells, causing the hydrogel to flow at conditions at which the high MW alginate remained gelated.

4.3. Printability

There is little consensus on the printing parameters of alginate-gelatin hydrogels in literature. Other investigations determine hydrogel printability using various methods such as Pr value, line uniformity, line spreading, and similarity to STL (Standard Tessellation Language) model files (Kiyotake et al., 2019). The hydrogel materials (alginate, gelatin, cellulose, etc.) are often the main factor considered when determining the printing parameters of these hydrogels. Here we examined the direct influence of cell concentration at varying degrees of magnitude and their effect on two similar but distinct hydrogels. It was observed that decreases in storage modulus and viscosity with increasing cell concentration correlate to the decreasing pressures needed to extrude these gels from a nozzle and the behavior of the gels exiting the nozzles. The decrease in pressure needed to print these samples was due to the decrease in gel stiffness caused by the incorporation of cells into the hydrogel, allowing the gels to flow with less force. Increasing cell concentration was found to negatively impact the structural properties of the extruded material by increasing line spreading post-print. We find that hydrogels composed of higher

molecular weight alginates and the highest initial cell-seeding densities (10^7 cells/mL) yield high structural uniformity.

4.4. Viability

The viability data did not support a systematic variation between the hydrogel compositions and seeding densities. We observed that seeding densities of 2×10^5 and 2×10^7 cells/mL displayed low viability of <65% for the high MW hydrogel one day after printing. Lower viability upon printing is attributed to the cells experiencing stresses and succumbing to damage. Also, as expected, the low viscosity hydrogel seeded at 2×10^5 and 2×10^7 cells/mL displayed higher viability, likely due to the lower pressure needed to print the gels, resulting in the cells within the gels experiencing less shear stresses. The high MW hydrogel with a seeding density of 1.5×10^6 cells/mL did not follow an expected viability pattern. The viability fluctuated considerably during the incubation period, with the incubation after five days being lower than the initial viability (approx. 50%). The viability of cells within the low MW alginate samples (2×10^5 and 2×10^7 cells/mL) and high MW samples (1.5×10^6 and 2×10^7 cells/mL) displayed high viability after five days of incubation. The high MW hydrogel with a seeding density of 1.5×10^6 cells/mL and the low MW hydrogel with a seeding density of 2×10^5 cells/mL had the best viability (>80%), which was slightly less than some similar studies have reported (Kiyotake et al., 2019). Even though the high MW hydrogel seeded with a concentration of 2×10^7 cells/mL did not yield the highest printability factor, cells within the gel still displayed high viability. Also, at 25 °C, the high MW hydrogel exhibited better printability versus low MW gels due to higher stiffness.

4.5. Limitations

The hydrogels are extremely sensitive to ambient conditions. As the syringe jacket of the bioprinter does not entirely cover the syringe containing the bioink, changes in lab temperature and pressure may have caused changes in the behavior of the hydrogel during printing. Further, temperature-controlled experiments are needed to determine the impact of ambient temperature fluxes on the stiffness and gelation time of these hydrogels. Similarly, the effects of temperature on printability with varying cell-seeding density, particularly for the low viscosity hydrogels, should be explored in more detail. Lower temperatures could lead to gelation of the seeded gels displaying enhanced printability. The exact mechanics of adding various cells to the hydrogels on the internal structure of the hydrogel is also unknown and needs further investigation.

5. Conclusions

Using varying molecular weight alginate-based hydrogels, this investigation explored how cell seeding density affects viscoelastic properties, printability, and cell viability. We found a distinct inverse relationship between the initial seeding density and the stiffness of the bio-ink. Increasing cell seeding density was shown to decrease the pressure needed to extrude intact hydrogel filaments. Conversely, a decrease in hydrogel stiffness was observed with increasing cell concentration which negatively impacted the structural properties of extruded material. To the best of our knowledge, a consistent relationship between cell seeding density and stiffness of hydrogel has not been observed. The observed differences in the relationship between seeding density and cell interactions with the hydrogel matrix could be a result of matrix variability and cell interactions with the hydrogel matrix. This resulted in an increase in filament spreading following extrusion. However, high molecular weight hydrogels allowed for the printing of high cell concentrations. of 2×10^7 cells/mL with greater than >80% viability after five days. By optimizing the printing parameters of the hydrogel, along with the alginate MW and seeding density, we were able to obtain printed structures with high viability and printability. The high MW bioink could be used for further studies to make models closer to the cell density of native tissues. In addition, the printability of hydrogels could be further investigated by tuning variables such as temperatures and nozzle size. Based on our observations, high seeding densities produce more numerous but smaller cell aggregates in a printed structure. These rapidly forming aggregates may facilitate faster rates of larger tissues. Future work should examine co-cultured cells to examine how multiple cell types impact hydrogel structure viscoelasticity over time. These investigations will expand knowledge on cell seeding density effects on printable biomaterials, advancing future rapid fabrication of functional tissue models for therapeutic screening.

CRediT authorship contribution statement

Tyler Gregory: Writing – review & editing, Writing – original draft, Visualization, Validation, Methodology, Investigation, Formal analysis, Data curation. **Prateek Benhal:** Writing – review & editing, Methodology, Investigation, Formal analysis, Data curation. **Annie Scutte:** Writing – review & editing, Methodology, Investigation, Formal analysis, Data curation. **David Quashie:** Writing – review & editing, Formal analysis, Data curation. **Kiram Harrison:** Writing – review & editing, Data curation. **Casey Cargill:** Writing – review & editing, Data curation. **Saliya Grandison:** Writing – review & editing, Data curation. **Mary Jean Savitsky:** Writing – review & editing, Data curation. **Subramanian Ramakrishnan:** Writing – review & editing, Validation, Supervision, Resources, Project administration, Methodology, Investigation, Funding acquisition, Formal analysis, Data curation, Conceptualization. **Jamel Ali:** Writing – review & editing, Writing – original draft, Supervision, Resources, Project administration, Methodology, Investigation, Funding acquisition, Formal analysis, Data curation, Conceptualization.

Declaration of competing interest

The authors declare that they have no known competing financial interests or personal relationships that could have appeared to influence the work reported in this paper.

Data availability

Data will be made available on request.

Acknowledgments

This work was funded by the National Science Foundation (No. HDR-2000202 and CMMI-2000330) and supported by the NSF FAMU CREST Center award (No. HDR-1735968). This research work was also supported by The Grainger Foundation Frontiers of Engineering Grant under the National Academy of Sciences Award Number: 2000013181 and the CaRE2 - REC Program, funded by the National Cancer Institute (NCI) of the National Institutes of Health (NIH) through the grants of NIH/NCI1U54CA233396, 1U54CA23344, and 1U54CA23346. Support was also provided by the National Institute Of General Medical Sciences of the National Institutes of Health under Award Number R16GM145595. All the work was performed at the National High Magnetic Field Laboratory, which is supported by National Science Foundation Cooperative Agreement No. DMR-1644779 and the State of Florida.

The content is solely the responsibility of the authors and does not necessarily represent the official views of The Grainger Foundation or the National Academy of Sciences.

Figs. 1 and 7 were made with Biorender (biorender.com).

References

Ahadian, S., Khademhosseini, A., 2018. A perspective on 3D bioprinting in tissue regeneration. Bio-Design Manuf. 1 (3), 157–160. https://doi.org/10.1007/s42242-018-0020-3.

Axpe, E., Oyen, M.L., 2016. Applications of alginate-based bioinks in 3D bioprinting. Int. J. Mol. Sci. 17 (12), 1976. https://doi.org/10.3390/ijms17121976.

Baker, B.M., Chen, C.S., 2012. Deconstructing the third dimension - how 3D culture microenvironments alter cellular cues. J. Cell Sci. 125 (13), 3015–3024. https://doi.org/10.1242/jcs.079509.

Bott, K., Upton, Z., Schrobback, K., Ehrbar, M., Hubbell, J.A., Lutolf, M.P., Rizzi, S.C., 2010. The effect of matrix characteristics on fibroblast proliferation in 3D gels. Biomaterials 31 (32), 8454–8464. https://doi.org/10.1016/j.biomaterials.2010.07.046.

Chung, J.H.Y., Naficy, S., Yue, Z.L., Kapsa, R., Quigley, A., Moulton, S.E., Wallace, G.G., 2013. Bio-ink properties and printability for extrusion printing living cells. Biomater. Sci. 1 (7), 763–773. https://doi.org/10.1039/c3bm00012e.

Di Giuseppe, M., Law, N., Webb, B., Macrae, R.A., Liew, L.J., Sercombe, T.B., Doyle, B.J., 2018. Mechanical behaviour of alginate-gelatin hydrogels for 3D bioprinting. J. Mech. Behav. Biomed. Mater. 79, 150–157. https://doi.org/10.1016/j.jmbbm.2017.12.018.

Diamantides, N., Dugopolski, C., Blahut, E., Kennedy, S., Bonassar, L.J., 2019. High density cell seeding affects the rheology and printability of collagen bioinks. Biofabrication 11 (4), 045016. https://doi.org/10.1088/1758-5090/ab3524.

Discher, D.E., Janmey, P., Wang, Y.L., 2005. Tissue cells feel and respond to the stiffness of their substrate. Science 310 (5751), 1139–1143. https://doi.org/10.1126/science.1116995.

Duval, K., Grover, H., Han, L.H., Mou, Y., Pegoraro, A.F., Fredberg, J., Chen, Z., 2017. Modeling physiological events in 2D vs. 3D cell culture. Physiology 32 (4), 266–277. https://doi.org/10.1152/physiol.00036.2016.

El-Rashidy, A.A., El Moshy, S., Radwan, I.A., Rady, D., Abbass, M.M.S., Dorfer, C.E., El-Sayed, K.M.F., 2021. Effect of polymeric matrix stiffness on osteogenic differentiation of mesenchymal stem/progenitor cells: concise review. Polymers 13 (17), 2950. https://doi.org/10.3390/polym13172950.

Gillispie, G.J., Han, A., Uzun-Per, M., Fisher, J., Mikos, A.G., Niazi, M.K.K., Atala, A., 2020. The influence of printing parameters and cell density on bioink printing outcomes. Tissue Eng. 26 (23–24), 1349–1358. https://doi.org/10.1089/ten.tea.2020.0210.

Gonzalez-Fernandez, T., Tenorio, A.J., Campbell, K.T., Silva, E.A., Leach, J.K., 2021. Alginate-based bioinks for 3D bioprinting and fabrication of anatomically accurate bone grafts. Tissue Eng. 27 (17–18), 1168–1181. https://doi.org/10.1089/ten.tea.2020.0305.

Guillotin, B., Souquet, A., Catros, S., Duocastella, M., Pippenger, B., Bellance, S., Guillemot, F., 2010. Laser assisted bioprinting of engineered tissue with high cell density and microscale organization. Biomaterials 31 (28), 7250–7256. https://doi.org/10.1016/j.biomaterials.2010.05.055.

Hickman, J.A., Graeser, R., de Hoogt, R., Vidic, S., Brito, C., Gutekunst, M., Consortium, I.P., 2014. Three-dimensional models of cancer for pharmacology and cancer cell biology: capturing tumor complexity in vitro/ex vivo. Biotechnol. J. 9 (9), 1115–1128. https://doi.org/10.1002/biot.201300492.

Holzl, K., Lin, S.M., Tytgat, L., Van Vlierberghe, S., Gu, L.X., Ovsianikov, A., 2016. Bioink properties before, during and after 3D bioprinting. Biofabrication 8 (3), 032002. https://doi.org/10.1088/1758-5090/8/3/032002.

Jensen, C., Teng, Y., 2020. Is it Time to Start Transitioning from 2D to 3D Cell Culture?, vol. 7 https://doi.org/10.3389/fmolb.2020.00033 [Review].

Kapalczynska, M., Kolenda, T., Przybyla, W., Zajaczkowska, M., Teresiak, A., Filas, V., Lamperska, K., 2018. 2D and 3D cell cultures - a comparison of different types of cancer cell cultures. Arch. Med. Sci. 14 (4), 910–919. https://doi.org/10.5114/aoms.2016.63743.

Kiyotake, E.A., Douglas, A.W., Thomas, E.E., Nimmo, S.L., Detamore, M.S., 2019. Development and quantitative characterization of the precursor rheology of hyaluronic acid hydrogels for bioprinting. Acta Biomater. 95, 176–187. https://doi.org/10.1016/j.actbio.2019.01.041.

Kuo, C.K., Ma, P.X., 2001. Ionically crosslinked alginate hydrogels as scaffolds for tissue engineering: Part 1. Structure, gelation rate and mechanical properties. Biomaterials 22 (6), 511–521. https://doi.org/10.1016/s0142-9612(00)00201-5.

Leberfinger, A.N., Dinda, S., Wu, Y., Koduru, S.V., Ozbolat, V., Ravnic, D.J., Ozbolat, I.T., 2019. Bioprinting functional tissues. Acta Biomater. 95, 32–49. https://doi.org/10.1016/j.actbio.2019.01.009.

Mandrycky, C., Wang, Z.J., Kim, K., Kim, D.H., 2016. 3D bioprinting for engineering complex tissues. Biotechnol. Adv. 34 (4), 422–434. https://doi.org/10.1016/j.biotechadv.2015.12.011.

Masuelli, M.A., Illanes, C.O., 2014. Review of the Characterization of Sodium Alginate by Intrinsic Viscosity Measurements: Comparative Analysis between Conventional and Single Point Methods.

Mauck, R.L., Wang, C.C.B., Oswald, E.S., Ateshian, G.A., Hung, C.T., 2003. The role of cell seeding density and nutrient supply for articular cartilage tissue engineering with deformational loading. Osteoarthritis Cartilage 11 (12), 879–890. https://doi.org/10.1016/j.joca.2003.08.006.

Mondal, A., Gebeyehu, A., Miranda, M., Bahadur, D., Patel, N., Ramakrishnan, S., Singh, M., 2019. Characterization and printability of Sodium alginate -Gelatin hydrogel for bioprinting NSCLC co-culture. Sci. Rep. 9, 19914. https://doi.org/10.1038/s41598-019-55034-9.

Moroni, L., Burdick, J.A., Highley, C., Lee, S.J., Morimoto, Y., Takeuchi, S., Yoo, J.J., 2018. Biofabrication strategies for 3D in vitro models and regenerative medicine. Nat. Rev. Mater. 3 (5), 21–37. https://doi.org/10.1038/s41578-018-0006-y.

Mota, C., Camarero-Espinosa, S., Baker, M.B., Wieringa, P., Moroni, L., 2020. Bioprinting: from tissue and organ development to in vitro models. Chem. Rev. 120 (19), 11032–11092. https://doi.org/10.1021/acs.chemrev.9b00789.

Moysidou, C.M., Barberio, C., Owens, R.M., 2021. Advances in engineering human tissue models. Front. Bioeng. Biotechnol. 8, 620962 https://doi.org/10.3389/fbioe.2020.620962.

Navaro, Y., Bleich-Kimelman, N., Hazanov, L., Mironi-Harpaz, I., Shachaf, Y., Garty, S., Gazit, Z., 2015. Matrix stiffness determines the fate of nucleus pulposus-derived stem cells. Biomaterials 49, 68–76. https://doi.org/10.1016/j.biomaterials.2015.01.021.

Ning, L.Q., Xu, Y.T., Chen, X.B., Schreyer, D.J., 2016. Influence of mechanical properties of alginate-based substrates on the performance of Schwann cells in culture. J. Biomater. Sci. Polym. Ed. 27 (9), 898–915. https://doi.org/10.1080/09205063.2016.1170415.

Ochando, J., Charron, D., Baptista, P.M., Uygun, B.E., 2017. Immun. respon. bioeng. organ. 22 (1), 79–85. https://doi.org/10.1097/mot.0000000000000378.

Ouyang, L.L., Yao, R., Zhao, Y., Sun, W., 2016. Effect of bioink properties on printability and cell viability for 3D bioplotting of embryonic stem cells. Biofabrication 8 (3), 035020. https://doi.org/10.1088/1758-5090/8/3/035020.

Pedde, R.D., Mirani, B., Navaei, A., Styan, T., Wong, S., Mehrali, M., Akbari, M., 2017. Emerging biofabrication strategies for engineering complex tissue constructs. Adv. Mater. 29 (19), 1606061 https://doi.org/10.1002/adma.201606061.

Rastogi, P., Kandasubramanian, B., 2019. Review of alginate-based hydrogel bioprinting for application in tissue engineering. Biofabrication 11 (4), 042001. https://doi.org/10.1088/1758-5090/ab331e.

Schwartz, R., Malpica, M., Thompson, G.L., Miri, A.K., 2020. Cell encapsulation in gelatin bioink impairs 3D bioprinting resolution. J. Mech. Behav. Biomed. Mater. 103, 103524 https://doi.org/10.1016/j.jmbbm.2019.103524.

Shafiee, A., Atala, A., 2016. Printing technologies for medical applications. Trends Mol. Med. 22 (3), 254–265. https://doi.org/10.1016/j.molmed.2016.01.003.

Szekalska, M., Pucilowska, A., Szymanska, E., Ciosek, P., Winnicka, K., 2016. Alginate: current use and future perspectives in pharmaceutical and biomedical applications, 2016 Int. J. Polym. Sci., 7697031. https://doi.org/10.1155/2016/7697031.

Vining, K.H., Mooney, D.J., 2017. Mechanical forces direct stem cell behaviour in development and regeneration. Nat. Rev. Mol. Cell Biol. 18 (12), 728–742. https://doi.org/10.1038/nrm.2017.108.

Wong, J.Y., Leach, J.B., Brown, X.Q., 2004. Balance of chemistry, topography, and mechanics at the cell-biomaterial interface: issues and challenges for assessing the role of substrate mechanics on cell response. Surf. Sci. 570 (1–2), 119–133. https://doi.org/10.1016/j.susc.2004.06.186.

Ye, K., Cao, L.P., Li, S.Y., Yu, L., Ding, J.D., 2016. Interplay of matrix stiffness and cell-cell contact in regulating differentiation of stem cells. ACS Appl. Mater. Interfaces 8 (34), 21903–21913. https://doi.org/10.1021/acsami.5b09746.

Zhang, J.H., Wehrle, E., Adamek, P., Paul, G.R., Qin, X.H., Rubert, M., Muller, R., 2020. Optimization of mechanical stiffness and cell density of 3D bioprinted cell-laden scaffolds improves extracellular matrix mineralization and cellular organization for bone tissue engineering. Acta Biomater. 114, 307–322. https://doi.org/10.1016/j.actbio.2020.07.016.

Zhang, W.D., Chu, G.L., Wang, H., Chen, S., Li, B., Han, F.X., 2020. Effects of matrix stiffness on the differentiation of multipotent stem cells. Curr. Stem Cell Res. Ther. 15 (5), 449–461. https://doi.org/10.2174/1574888x15666200408114632.